Pure Appl. Geophys.

https://doi.org/10.1007/s00024-020-02532-x

Pure and Applied Geophysics

Evidence-Calibrated Numerical Model of December 22, 2018, Anak Krakatau Flank Collapse and Tsunami

R. Omira[1,2] and I. Ramalho[1,2]

Abstract—On December 22, 2018, a sector of the Anak Krakatau volcano edifice collapsed into the sea, generating a tsunami that hit the Sunda Strait coasts in Indonesia. The collapse followed a period of 6 months of volcanic activity that was insufficient to warn the tsunami-threatened coastal population. The Anak Krakatau tsunami resulted in hundreds of casualties, thousands of injured and displaced people, and massive coastal damage. This paper uses the tsunami records, the collected field survey data, and satellite imagery-based interpretations to develop a model of the Anak Krakatau flank failure and tsunami. We address the dynamics of the flank failure, the tsunami generation and propagation, and the coastal impact using evidence-calibrated numerical modelling. An in-house-developed multi-layer viscoplastic shallow-water numerical code is employed to simulate the Anak Krakatau collapse mass movement and the whole source-to-coast tsunami process. Our results suggest that a flank collapse scenario involving a volume of material of 0.135 km^3 and occurring as a sequence of two failures fairly reproduces the local and regional tsunami records and survey data.

Keywords: Anak Krakatau volcano, tsunami, flank collapse, numerical modelling, Indonesia.

1. Introduction

Indonesia is probably the most tsunami-prone of the Indian Ocean countries, with one of the most highly tsunami-vulnerable coasts in the world (Løvholt et al. 2014). Tsunami hazard on the Indonesian coasts is mainly associated with large earthquakes that often occur within the active subduction zones and crustal faults (Horspool et al. 2014). The December 26, 2004, event that took place off Sumatra on Sunda Arc is an example of a megathrust earthquake and tsunami that devastated the Indonesian coast, along with many other countries of the Indian Ocean, killing over 230,000 people (Titov et al. 2005). Since the devastating 2004 event, Indonesia has experienced several moderate-to-large tsunamigenic earthquakes that continuously threaten its coastal community. More recently, on September 28, 2018, a massive tsunami followed the Mw7.5 Sulawesi earthquake that ruptured a 180-km-long strike-slip crustal fault (Socquet et al. 2019; Heidarzadeh et al. 2018). The 2018 Sulawesi earthquake and tsunami caused over 2000 fatalities (ASEAN 2018), and wave runup heights exceeded 7 m inside the Bay of Palu (Omira et al. 2019; Mikami et al. 2019).

Compared with tsunamis of seismic origin, volcanic tsunamis are considered rare. Nevertheless, they have occurred worldwide within distinct volcanic provinces and have been responsible for over 55,000 fatalities since 1600 (Auker et al. 2013; Williams et al. 2019). Indonesia hosts one of these critical volcanic provinces, which accounts for several past volcanic tsunamis (Paris et al. 2014). Among these events, the 1883 Krakatau remains the most devastating and deadly volcanic tsunami in recorded history. This tsunami event has been investigated extensively, yet its generation mechanism is still controversial, and several processes may have acted in succession or together (Latter 1981; Yokoyama 1987; Francis 1985; Nomanbhoy and Satake 1995; Carey et al. 2000; Choi et al. 2003; Maeno and Imamura 2011). The controversy over the 1883 tsunami source evidences the complexity of the generation mechanism of volcanic tsunamis that can involve volcano-tectonic earthquakes, slope

[1] Dom Luíz Institute (IDL), Faculty of Science, University of Lisbon, Lisbon, Portugal. E-mail: raomira@fc.ul.pt
[2] Portuguese Institute for Sea and Atmosphere (IPMA), Lisbon, Portugal.

Published online: 16 June 2020

instabilities, pyroclastic flows, underwater explosions, shock waves, and caldera collapse (Paris 2015).

Anak Krakatau volcano, lying in the Sunda Strait between Sumatra to the northwest and Java to the southeast (Fig. 1a, b), was formed following the major 1883 Krakatau eruption. Morphologically, Anak Krakatau is partly built on a steep wall of the 1883 caldera, making it prone to flank collapse occurrence (Paris et al. 2014) (Fig. 1c). Since 1928, when it first emerged above sea level (Giachetti et al. 2012), Anak Krakatau has experienced continuous stages of construction and destruction evidenced by numerous eruption episodes. On December 22, 2018, the growth of the volcanic island was interrupted by a massive eruption, leading to the destruction of a large sector of the volcano edifice. Consequently, a flank collapsed into the sea and generated a tsunami that struck the surrounding coasts of Sunda Strait. The tsunami waves caused over 400 fatalities, injured tens of thousands of people, and inflicted massive damage to thousands of homes, businesses, and boats (Putra et al. 2020; Takabatake et al. 2019).

The tsunami that followed the December 22, 2018, Anak Krakatau volcano eruption has been thoroughly investigated by several research groups. The published works include tsunami field surveys (Muhari et al. 2019; Takabatake et al. 2019; Putra et al 2020; Borrero et al. 2020), analysis of tsunami records (Muhari et al. 2019), interpretation of satellite images (Williams et al. 2019), analysis of seismic signals (Walter et al. 2019), and numerical models of flank collapse and subsequent tsunami propagation (Grilli et al. 2019; Heidarzadeh et al. 2020; Paris et al. 2020; Borrero et al. 2020). While these studies provide rich data offering a unique opportunity to better understand the volcanic tsunami hazard, the generation mechanism of the Anak Krakatau tsunami is still uncertain. This uncertainty is clearly evidenced in the different volume estimates for the collapse material as suggested by various studies. Grilli et al. (2019) used numerical modelling to demonstrate that a volume of 0.22–0.30 km^3 is needed to reproduce the recorded and observed tsunami. Similarly, Heidarzadeh et al. (2020) reported a volume in the range of 0.175–0.326 km^3. Paris et al. (2020) conducted numerical simulations of tsunami propagation but suggested that a smaller volume of 0.15 km^3 would be enough to generate the Anak Krakatau tsunami. Williams et al. (2019) reconstructed the tsunamigenic

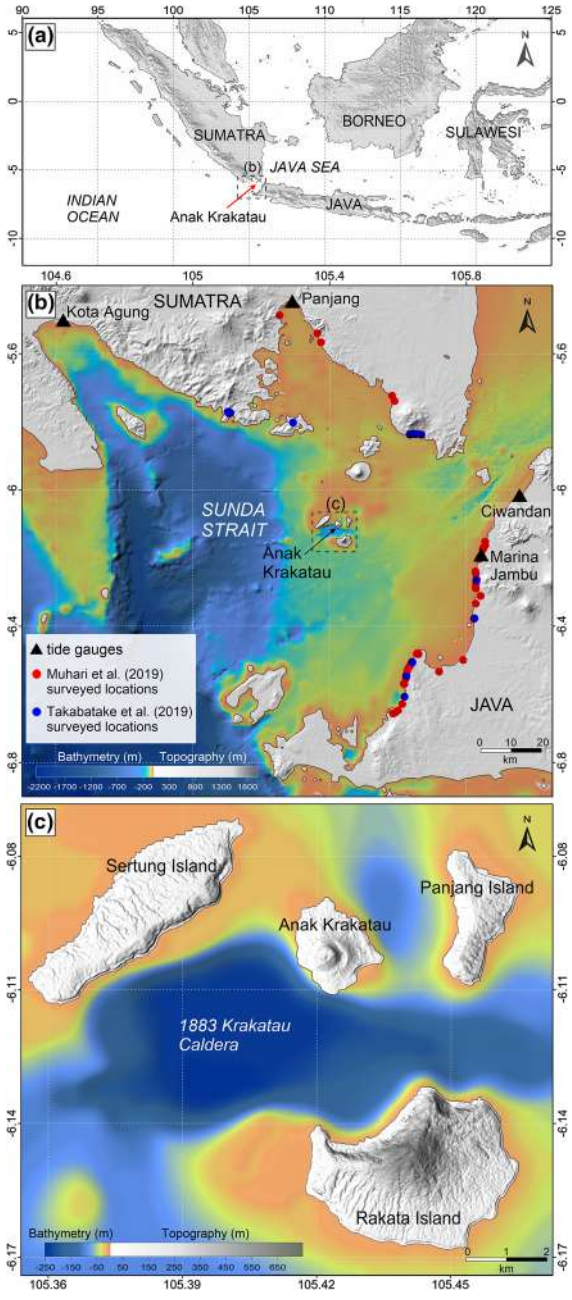

Figure 1
Location maps of Anak Krakatau volcano: **a** overview of the Anak Krakatau location between Sumatra and Java islands in Indonesia; **b** location of Anak Krakatau volcano within the Sunda Strait where the tsunami was recorded by coastal tide gauges (black triangles) and surveyed at Sumatra and Java coasts (red and blue dots); **c** digital elevation model of the 1883 Caldera, including Anak Krakatau and surrounding islands

flank collapse through a careful satellite imagery-based analysis, suggesting that a much smaller volume of 0.07 km^3 was involved in the tsunami generation.

This paper explores the generation mechanism, propagation, and hazard extent of the Anak Krakatau tsunami. It uses the available post-tsunami data together with numerical modelling to infer a flank collapse scenario that fairly reproduces the tsunami observations.

2. *Anak Krakatau Flank Collapse and Tsunami Models*

2.1. *Failure Model*

The failure mechanism of the flank collapse is a key element in the volcanic tsunami generation process. Whether the flank occurs in one-go collapse or as a sequence of multiple failures strongly influences the formation of the first wave when the involved material plunges into the sea. Here, we explore the hypothesis that the Anak Krakatau flank collapse occurred as a sequence of two failures. We infer this scenario from both eyewitness testimony (Prasetya et al. 2019) and satellite imagery analysis (Williams et al. 2019). We hypothesize that the Anak Krakatau flank was first initiated by the collapse of the lateral edifice, followed by the failure of the roof of the volcano (Fig. 2). Figure 2 depicts the morphological analysis of the Anak Krakatau volcano edifice based on Sentinel-1A satellite images captured before (Fig. 2a) and ∼ 8 h after the tsunami (Fig. 2b). The inferred flank collapse scenario (Fig. 2c) is consistent with both the testimony of eyewitnesses, who described seeing the island "divided into two and immediately followed by the peak collapse, which resulted in more than one wave" (Prasetya et al. 2019), and the interpretation performed by Williams et al. (2019).

To build the Anak Krakatau failure scenario, we gathered the best available topographic and bathymetric data enabling the compilation of a high-resolution digital elevation model (DEM) at the tsunami generation area. We obtained the topographic data from DEMNAS (https://tides.big.go.id/DEMNAS/index.html) with 10 m horizontal resolution. For the bathymetric data, the Indonesian Geospatial Information Agency (BIG) (https://big.go.

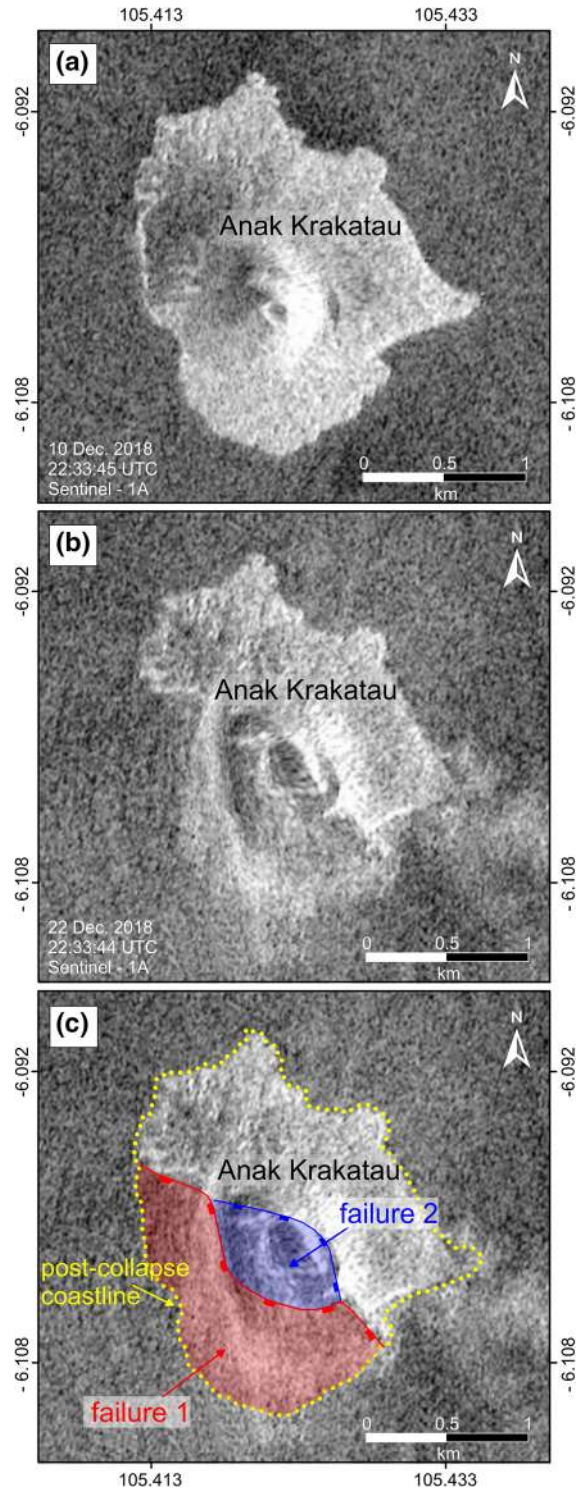

◀Figure 2
Analysis of Anak Krakatau flank collapse morphology: **a** satellite image of Anak Krakatau volcano captured by Sentinel 1A before the tsunami event, on December 10, 2018; **b** satellite image of Anak Krakatau volcano captured by Sentinel 1A ∼ 8 h after the tsunami event, on December 22, 2018; **c** interpretation of the Anak Krakatau flank collapse that generated the tsunami

id) provided a pre-event 5-m-resolution grid of the 1833 caldera. The compilation of these data allowed us to construct a 10-m-resolution DEM that enabled a better representation of both bathymetric and topographic features of Anak Krakatau volcano and surrounding islands (Figs. 1c, 3a).

During the failure process, the volume of the material involved strongly influences the tsunami generation and, therefore, the level and extent of the associated hazard. Accurate evaluation of flank collapse-induced tsunamis requires precise determination of the volume of the material involved. Here, due to the lack of post-event bathymetry data and seismic profiles that would allow us to determine the mass-wasting deposit, we are only able to speculate about the collapsed volume. Using basic morphologic analysis, we infer a volume of ∼ 0.1 km^3 for failure 1, corresponding to the collapse of the lateral sector of Anak Krakatau volcano edifice (Fig. 3b), and a volume of ∼ 0.035 km^3 for the collapse of the volcano roof (failure 2, Fig. 3c). The failure 1 scenario is consistent with the volume suggested by Williams et al. (2019). For a collapse involving both failures 1 and 2 (Fig. 3d), we obtain a volume of ∼ 0.135 km^3, which is similar to the volume estimate by Paris et al. (2020) and close to the lower volume range estimate of Heidarzadeh et al. (2020). On the other hand, our estimate of the Anak Krakatau collapse volume is approximatly half the size of that suggested by Grilli et al. (2019).

2.2. *Tsunami Numerical Model*

To simulate the Anak Krakatau collapse and the wave induced by its mass entering the water, we employ a multi-layered viscoplastic shallow-water model solved in a finite volume scheme. In this in-house-developed numerical code, the landslide dynamics are governed by the viscoplastic Bingham model, a simplified Herschel–Bulkley rheology model (Jiang and LeBlond 1993; Huang and Garcia 1998; Imran et al. 2001), and the wave generation and propagation are approximated by the non-linear shallow-water equations. The viscoplastic Bingham rheological model expresses the one-dimensional stress–strain relation as follows:

$$\begin{cases} \frac{\partial u}{\partial z} = 0, & \tau < \tau_0 \\ \frac{\partial u}{\partial z} = \frac{1}{\mu}(\tau - \tau_0), & \tau > \tau_0 \end{cases}, \quad (1)$$

where $\frac{\partial u}{\partial z}$ is the shear rate, u is the horizontal flow velocity, z is the vertical axis positive upward, τ is the shear stress, τ_0 is the yield (or Bingham) stress, and μ is the coefficient of dynamic viscosity.

In this study, we use De Blasio et al. (2005) formulation to account for the time variation of the yield stress:

$$\tau_0(\gamma) = \tau_{0,t=\infty} + \left(\tau_{0,t=0} - \tau_{0,t=\infty}\right)\mathrm{e}^{-\Gamma\gamma}, \quad (2)$$

where γ is the total shear deformation, $\tau_{0,t=0}$ and $\tau_{0,t=\infty}$ are the initial and residual yield stresses, and Γ is a dimensionless coefficient to quantify the efficiency in the strength loss. For the Anak Krakatau collapse movement we considered $\tau_{0,t=0} = 50$ kPa, $\tau_{0,t=\infty} = 20$ kPa, and $\Gamma = 0.0005$.

In a viscoplastic model, the landslide layer is composed of two distinct zones: a shear deformable zone of thickness D_s, and a non-deformable plug zone of thickness D_p. In this paper, we follow the Skvortsov and Bornhold (2007) formulation of continuity and momentum equations allowing the entire landslide thickness (D) to be determined by introducing a relative thickness ($d1$, see Eq. 3), instead of the classical approach of solving two separate systems of equations involving both thicknesses D_s and D_p (Jiang and LeBlond 1993; Imran et al. 2001). Additionally, we ensure that the equations governing the landslide dynamics integrate a realistic presentation of the bathymetry slopes and the landslide subaerial part, following Fine et al. (2003) and Thomson et al. (2001).

The dynamics of the landslide body and the generation and propagation of the subsequent tsunami are respectively governed by the systems of Eqs. (3) and (4), expressed in Cartesian coordinates as follows:

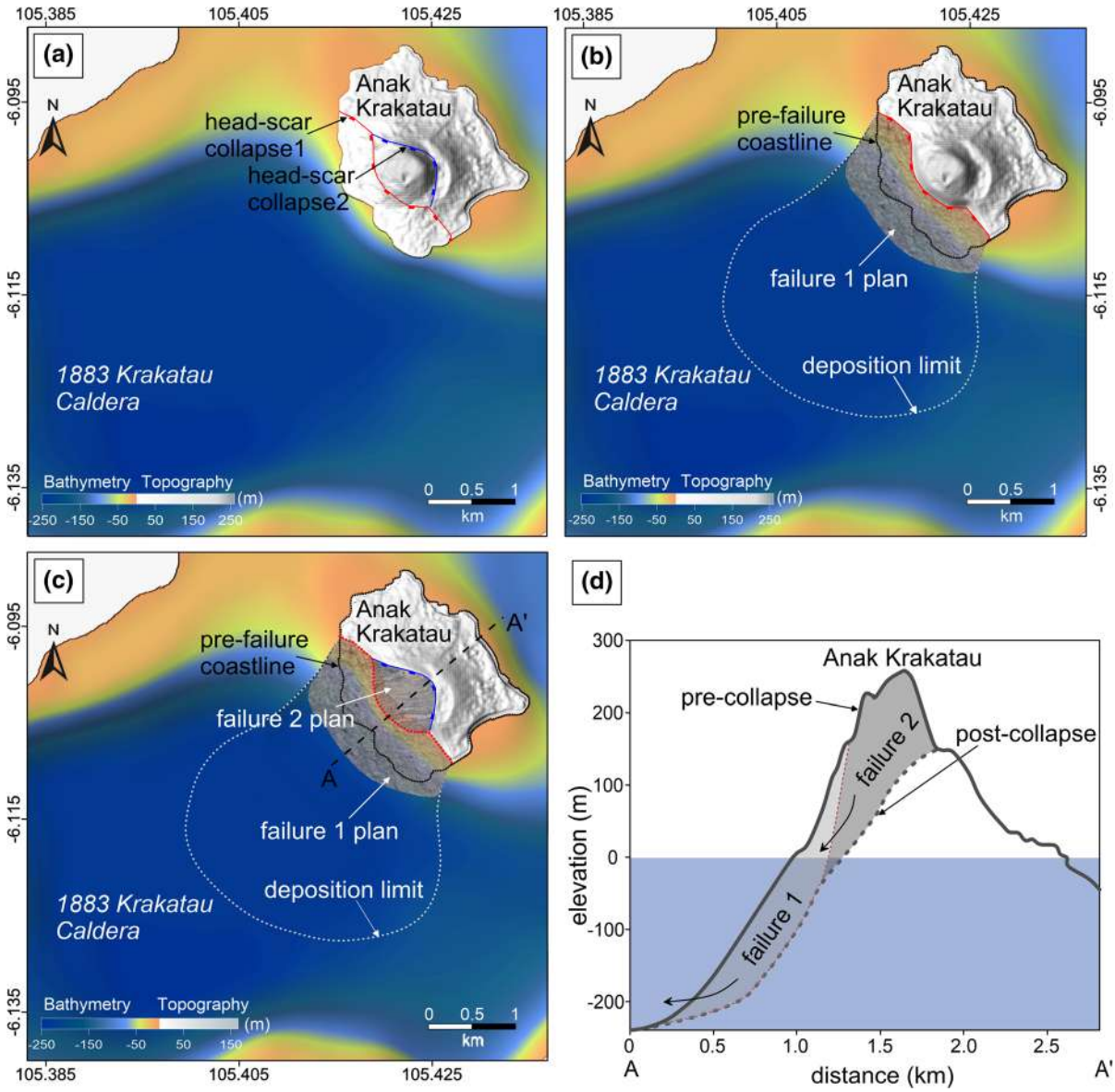

Figure 3

Anak Krakatau flank failure model: **a** head-scars of failures 1 and 2 within the Anak Krakatau topography; **b** failure 1 plan identification within the Anak Krakatau volcano; **c** failure 2 plan identification within the Anak Krakatau volcano; **d** cross-section of the flank collapse model including both failures 1 and 2

$$
\begin{aligned}
&\frac{\partial D}{\partial t}+\frac{\partial UD}{\partial x}+\frac{\partial VD}{\partial y}=0,\\
&\frac{\partial UD}{\partial t}+\frac{\partial \alpha U^2 D}{\partial x}+\frac{\partial \alpha UVD}{\partial y}\\
&=-\frac{g}{\rho_2}\left[(\rho_2-\rho_1)D\left(\frac{\partial D}{\partial x}-\frac{\partial h_s}{\partial x}\right)+\rho_1\frac{\partial \eta}{\partial x}\right]\\
&-\frac{1}{\rho_2}\left[\frac{U}{\overline{U}}\tau_0(1+d_1)+\frac{2\mu U}{D\left(1-\frac{d_1}{3}\right)}\right],\\
&\frac{\partial VD}{\partial t}+\frac{\partial \alpha UVD}{\partial x}+\frac{\partial \alpha V^2 D}{\partial y}\\
&=-\frac{g}{\rho_2}\left[(\rho_2-\rho_1)D\left(\frac{\partial D}{\partial y}-\frac{\partial h_s}{\partial y}\right)+\rho_1\frac{\partial \eta}{\partial y}\right]\\
&-\frac{1}{\rho_2}\left[\frac{V}{\overline{U}}\tau_0(1+d_1)-\frac{2\mu V}{D\left(1-\frac{d_1}{3}\right)}\right],
\end{aligned}
\tag{3}
$$

$$
\begin{aligned}
&\frac{\partial(h_s+\eta-D)}{\partial t}+\frac{\partial(h_s+\eta-D)u}{\partial x}\\
&+\frac{\partial(h_s+\eta-D)v}{\partial y}=0,\\
&\frac{\partial u}{\partial t}+u\frac{\partial u}{\partial x}+v\frac{\partial u}{\partial y}=-g\frac{\partial \eta}{\partial x},\\
&\frac{\partial v}{\partial t}+u\frac{\partial v}{\partial x}+v\frac{\partial v}{\partial y}=-g\frac{\partial \eta}{\partial y},
\end{aligned}
\tag{4}
$$

where D is the thickness of the landslide; η is the water free surface displacement; h_s is the static water depth (bathymetry); u, v, U, V are the horizontal components of the velocities in the x- and y-directions of the wave and the landslide, respectively; g is the gravity acceleration; ρ_1 and ρ_2 are the densities of the water and the landslide, respectively; $d_1 = \sqrt{k^2+2k}-k$ is the shear layer relative to total thickness; $k=\frac{\mu|\overline{U}|}{\tau_0 D\left(1-\frac{d_1}{3}\right)}$ is the viscoplastic ratio $(0<k<\infty)$; $\propto=\frac{1-\frac{7}{15}d_1}{\left(1-\frac{d_1}{3}\right)^2}$ is a coefficient constrained between $1<\propto<1.2$; and $\overline{U}=\sqrt{U^2+V^2}$ is the full speed.

3. Results and Discussion

3.1. Anak Krakatau Tsunami Generation

We simulate the dynamics of the Anak Krakatau flank collapse and the resulting tsunami generation (Fig. 4). Here, the Anak Krakatau collapse is assumed to occur as a sequence of two failures (failure 1 and failure 2, Fig. 3), with a time lag of 5.0 s. Such a short time lag is considered to match the eyewitnesses testimony, reporting an immediate collapse of the volcano roof following the lateral failure. At t = 0 s, the lateral flank (failure 1), with an estimated volume of $\sim$ 0.1 km^3, is initiated and starts moving downslope (Fig. 4a). It is immediately (after 5 s) followed by the collapse of the volcano roof (failure 2), volume $\sim$ 0.035 km^3, that rapidly plunges into the sea (Fig. 4b). The material removed from both failures moves rapidly down the steep slope (Fig. 4c) and reaches a steady state after 75 s (Fig. 4d). At this stage, the simulated dynamics of the Anak Krakatau flank collapse suggest a material deposit spreading over an area of $\sim$ 7.5 km^2 within the Krakatau caldera, with a maximum runout distance of about 2.8 km. These results are in good agreement with the data obtained from the preliminary post-event bathymetric survey that showed the presence of collapse deposits extending at similar runout distances (Muhari et al. 2019).

The Anak Krakatau tsunami is initiated immediately following the collapse of the lateral flank (failure 1) that perturbs the nearshore water, leading to the formation of a wave of about 25 m in height (Fig. 4f). The formed tsunami continues growing and propagating away from the Anak Krakatau shoreline, while the landslide from both failures is moving downslope and pumping the energy into the wave (Fig. 4g). During the tsunami generation phase, we observe that the landslide and the formed wave move at approximately the same speed (Fig. 4), suggesting possible resonance interaction between the two moving layers. At t = 75 s, with the landslide in its steady state, the tsunami generation process is completed with the formation of a large wave of about 45 m in height (Fig. 4h). The results obtained by Heidarzadeh et al. (2020) and Paris et al. (2020) estimated an initial tsunami wave with height of 100 m and 80 m, respectively.

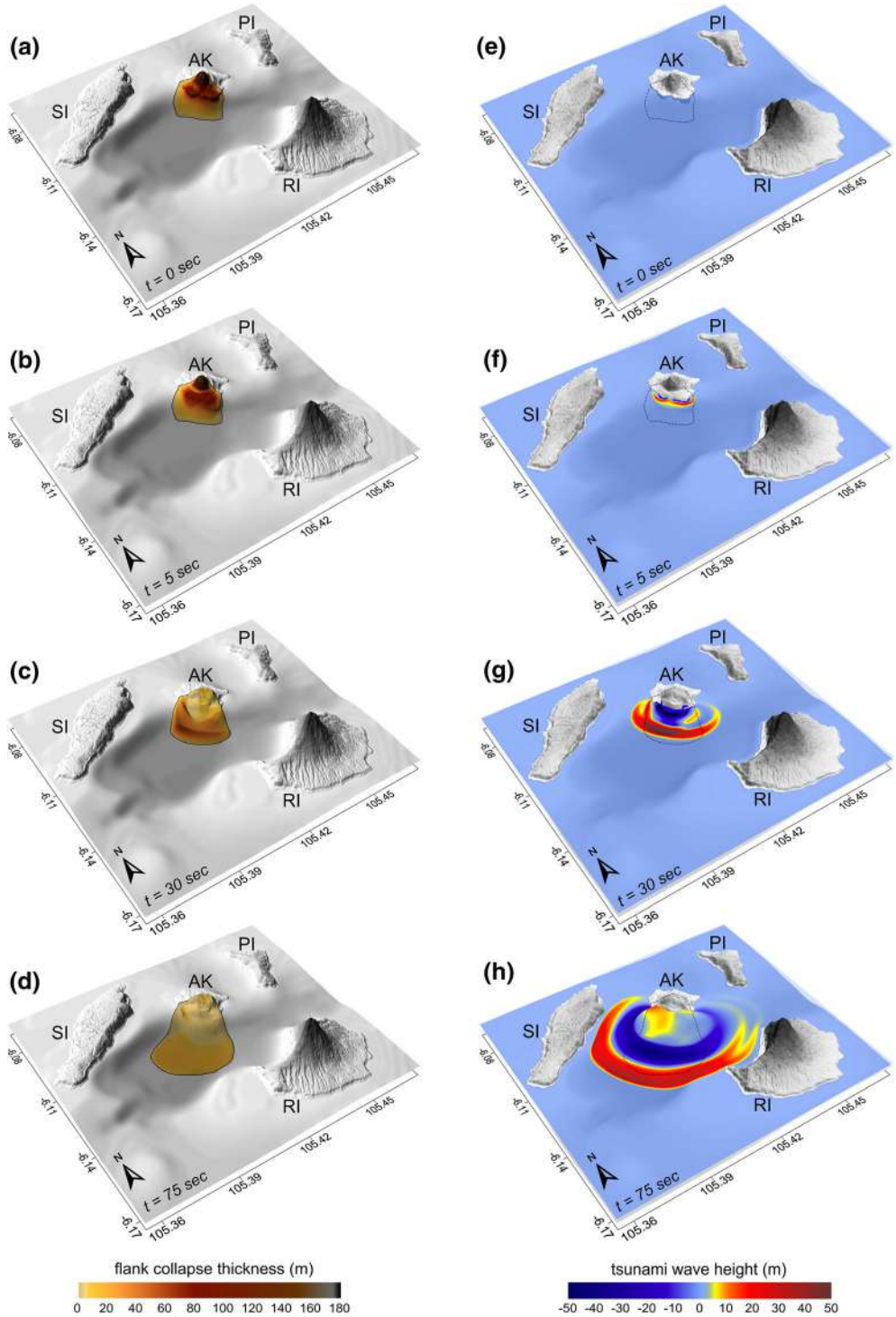

Figure 4

Simulations of Anak Krakatau flank collapse dynamics and tsunami generation: **a**–**d** snapshots of the downslope mass failure movement; **e**–**h** snapshots of tsunami generation, with dashed contours marking the flank failure limits. *AK* Anak Krakatau, *SI* Sertung Island, *PI* Panjang Island, *RI* Rakata Island

3.2. *Anak Krakatau Tsunami Propagation and Hazard Extent*

We simulate the propagation over the Sunda Strait of the Anak Krakatau tsunami from its source to both the Sumatra and Java coasts. Our simulations provide the synthetic waveforms at coastal tide gauge locations that recorded the tsunami signal, the maximum wave height distribution in Sunda Strait, and the tsunami inundation, flow depths, and runup heights at the islands surrounding Anak Krakatau, where tsunami observations are available. We then analyse and compare the obtained results with recorded, surveyed, and observed data from the Anak Krakatau tsunami.

Figure 5 depicts the computed waveforms plotted together with the tsunami records from four coastal tide gauges, namely Marina Jambu (Fig. 5a) and Ciwandan (Fig. 5b) at the Java coast (Fig. 2b, for location), and Kota Agung (Fig. 5c) and Panjang (Fig. 5d) at the Sumatra coast (Fig. 2b, for location). Overall, the numerical simulation results fairly reproduce most of the signals recorded at the tide gauges, particularly regarding the maximum height of the tsunami and its arrival time. Recorded versus modelled heights of the first higher wave, respectively, show 1.33 m vs. 1.34 m at Marina Jambu (Fig. 5a), 0.37 m vs. 0.32 m at Ciwandan (Fig. 5b), 0.32 m vs. 0.21 m at Kota Agung (Fig. 5c), and 0.34 m vs. 0.15 m at Panjang (Fig. 5d). Arrival time also shows some differences between simulated and recorded tsunami signals, with delays of $\sim$ 1 min at Kota Agung and 2.3 min at Ciwandan (Fig. 5). Despite the differences in volume estimates and collapse mechanisms, the simulations presented in the research articles by Grilli et al. (2019) and Paris et al. (2020) show similar disagreements in arrival times and wave heights between the modelled tsunami waveforms and the recorded signals. We

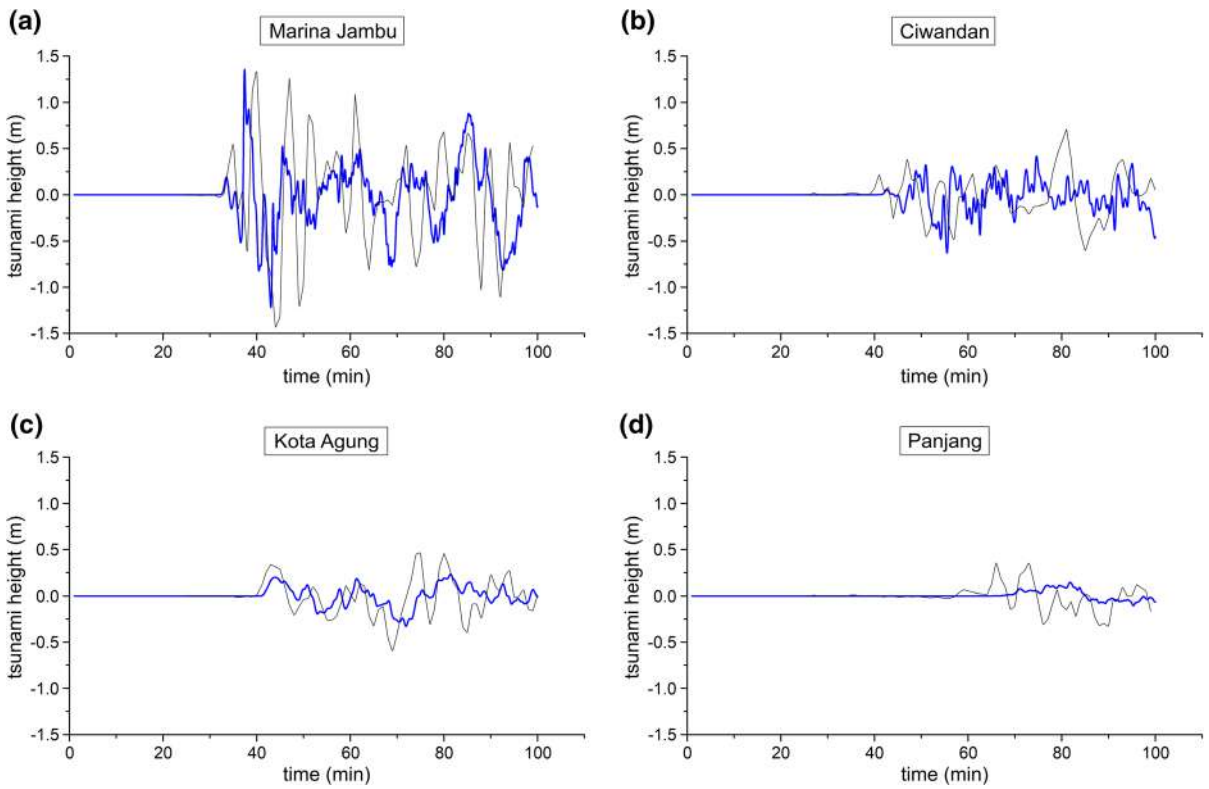

Figure 5
Comparison between recorded (in black) and simulated (in blue) tsunami wave heights at tide gauge stations of **a** Marina Jambu, **b** Ciwandan, **c** Kota Agung, and **d** Panjang

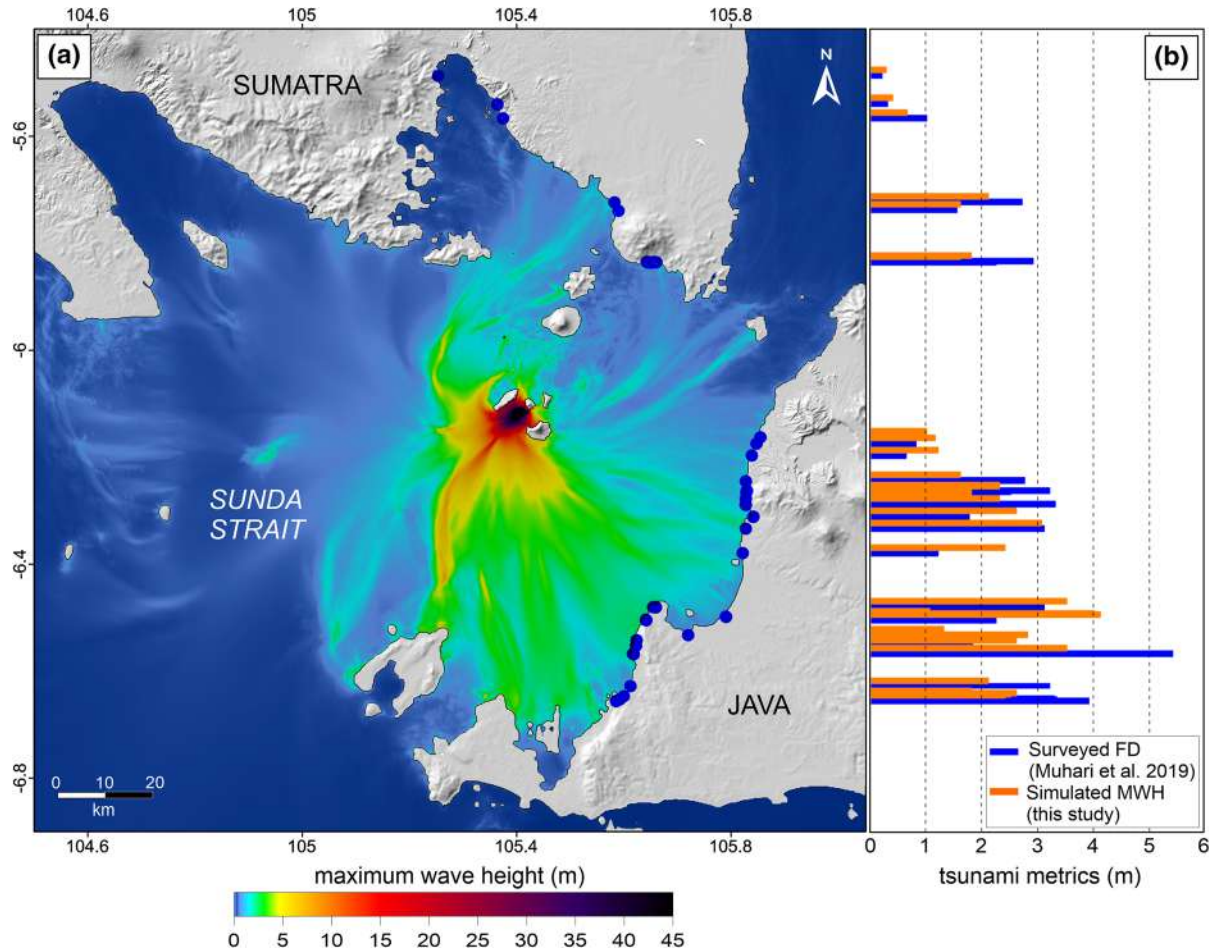

Figure 6

Regional Anak Krakatau tsunami hazard extent: **a** maximum tsunami wave height simulated in Sunda Strait; **b** comparison between field survey flow depth (FD) (blue bars) and simulated maximum wave height (MWH) (orange bars) at survey coastal locations (blue dots in **a**)

believe that the quality of the nearshore bathymetric data used here strongly affects the modelling results, leading to the inconsistency between the synthetic and recorded waveforms.

To provide insight into the extent of the Anak Krakatau tsunami hazard, we present the overall distribution of maximum wave heights within the Sunda Strait (Fig. 6). Figure 6a suggests that the Anak Krakatau tsunami reached the coast of Java with higher waves than those reaching the coast of Sumatra. These results are in good agreement with the field survey results that reveal a higher tsunami impact in Java than in Sumatra (Muhari et al. 2019) (Fig. 6b). Analysis of the results illustrated in Fig. 6a also indicates that the tsunami wave underwent significant dissipation when travelling from the source area towards the coasts of both Java and Sumatra. Within the volcano caldera, the tsunami wave is as high as 45 m. Tens of kilometres away from the source area, the tsunami wave heights are noticeably attenuated when reaching the coasts of Java and Sumatra (Fig. 6). Significant dissipation of wave energy is a common characteristic of tsunamis caused by non-seismic sources, such as submarine landslides or flank collapses. Such point-source tsunamis often cause high local but limited regional and far-field impact.

Locally, the Anak Krakatau volcano is surrounded by three other volcanic islands, namely Sertung (northwest), Rakata (southeast), and Panjang (northeast) (Fig. 1c, for location). On both islands facing the collapse (Sertung and Rakata), the Anak Krakatau

tsunami has left clear inundation marks on the coastal vegetation, enabling the estimate of runup height (Muhari et al. 2019; Paris et al 2020). Muhari et al. (2019) report runup height of 15 m at Rakata and up to 40 m at Sertung, while Paris et al.'s (2020) estimates are in the range of 25–30 m for both islands. Simulations of the inundation, including flow depths and runup heights, resulting at the Sertung and Rakata coasts from the Anak Krakatau tsunami are depicted in Fig. 7. These results evidence the high tsunami impact on the island coasts facing the source area. Here, the modelled maximum flow depth reaches 45 m at Sertung and 30 m at Rakata (Fig. 7a, b), and the runup is up to 60 m in height (Fig. 7c, d). Simulated runup heights at aerial survey locations (see Fig. 7) show values in the range of 18–45 m at the Sertung coast and 15–30 m at the Rakata coast (Fig. 7c, d). These values are consistent with runup heights reported by Muhari et al. (2019) and Paris et al. (2020).

It is clear from both the local (Figs. 4, 7) and regional (Figs. 5, 6) tsunami hazard modelling results

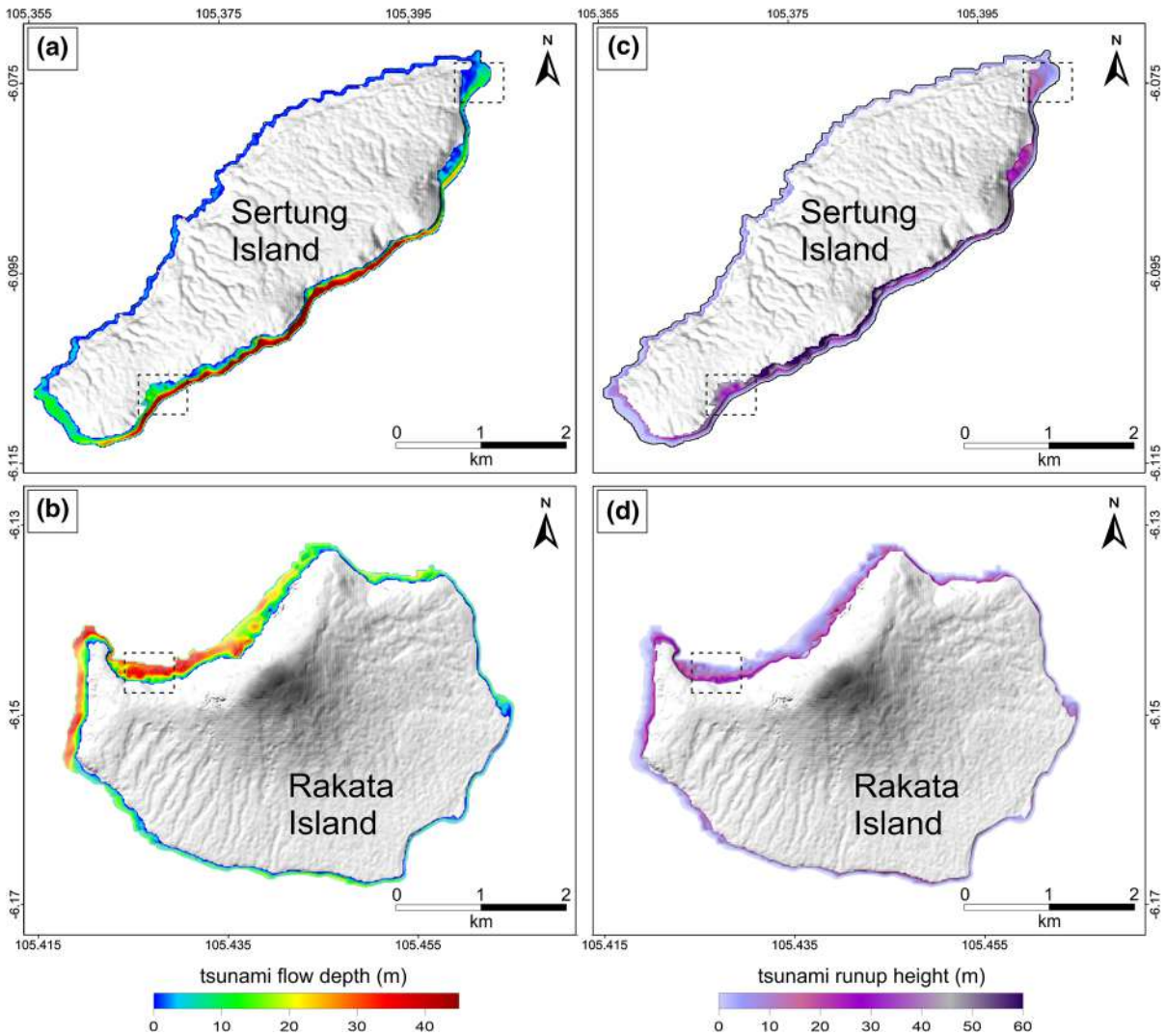

Figure 7
Local tsunami coastal impact: **a** Sertung Island inundation flow depth map; **b** Rakata Island inundation flow depth map; **c** Sertung Island runup height map; **d** Rakata Island runup height map. Dashed rectangles mark the locations of the aerial survey

that the focus of the tsunami energy is within the Anak Krakatau-Sertung-Rakata basin. Islands of this basin serve as natural protective barriers against the propagation of a highly energetic tsunami towards the coasts of Java and Sumatra. The relatively low tsunami energy that reached these coasts resulted from the waves escaping the Anak Krakatau-Sertung-Rakata basin. A similar effect of a semi-enclosed basin on the extent of volcanic tsunami hazard was reported in the volcanic archipelago of Azores, NE Atlantic region (Omira et al. 2016).

It is worth mentioning here that despite the satisfactory numerical results obtained using the two-stage Anak Krakatau flank collapse, the hypothesis of one-go collapse cannot be ruled out. Previous studies that considered a one-stage Anak Krakatau flank collapse also show simulation results in good agreement with the tsunami observations (Grilli et al. 2019; Paris et al. 2020). Further investigation of the post-collapse deposit, through acquisition of high-resolution bathymetric and seismic data, could help provide important insight into the failure mechanism of the Anak Krakatau flank.

4. Conclusions

The tsunami that followed the December 22, 2018, Anak Krakatau eruptive activity evidenced the potential of ocean volcanic islands in generating major sea waves. Nevertheless, it illustrated the limitation of tsunami warning systems in dealing with volcano events and brought to the fore the complexity of the volcanic tsunami´s generation mechanism. In this paper, we explore the Anak Krakatau failure mechanism and the induced tsunami generation and propagation at both local and regional scales. We use the best available Anak Krakatau post-event data, namely the tsunami recorded and survey data, to calibrate the numerical models employed to simulate the dynamics of the flank collapse and the source-to-coast tsunami propagation and coastal impact.

In conclusion, we summarize the main findings of this study as follows:

1. We propose a flank failure scenario consistent with eyewitness testimony and satellite imagery interpretation, which involves a volume of 0.135 km^3, occurring as a sequence of two failures.
2. The 0.135-km^3 volume flank collapse allows for simulating tsunami waves that reproduce quite well the post-event Anak Krakatau tsunami data.
3. Comparison between the simulated and recorded waveforms shows some dissimilarities in arrival time and wave height, which may be attributed to the quality of the nearshore bathymetry data used in the modelling.
4. The numerical results evidence the high local and limited regional tsunami impact of the Anak Krakatau tsunami, a common characteristic of non-seismic tsunamis.
5. The islands surrounding the Anak Krakatau volcano may have played a role as natural protective barriers preventing the propagation of higher tsunami waves towards the coasts of Java and Sumatra.

Acknowledgements

This work is funded by the project MAGICLAND (Fundação para a Ciência e Tecnologia (FCT), Portugal; PTDC/CTA-GEO/30381/2017). R. Omira acknowledges his CEECIND/04876/2017 researcher contract funded by Fundação para a Ciência e a Tecnologia (FCT), Portugal. The authors acknowledge the financial support of FCT through project UIDB/50019/2020 – IDL. The authors thank Gegar Prasetya and Rebecca Williams for the fruitful discussion on the collapse mechanism. The authors also wish to thank the Editor-in-Chief Alexander Rabinovich and the two anonymous reviewers for their timely and helpful reviews, which improved the manuscript.

References

ASEAN. (2018). ASEAN-Coordinating Centre for Humanitarian Assistance on disaster: Situation Update No. 12 M 7.4

Earthquake & Tsunami Sulawesi, Indonesia. https://asean.org/storage/2018/10/AHA-Situation_Update-no12-Sulawesi-EQ-rev.pdf. Accessed Jan 2020.

Auker, M. R., Sparks, R. S. J., Siebert, L., Crosweller, H. S., & Ewert, J. (2013). A statistical analysis of the global historical volcanic fatalities record. *Journal of Applied Volcanology, 2*(1), 2. https://doi.org/10.1186/2191-5040-2-2.

Borrero, J. C., Solihuddin, T., Fritz, H. M., et al. (2020). Field survey and numerical modelling of the December 22, 2018 Anak Krakatau Tsunami. *Pure and Applied Geophysics*. https://doi.org/10.1007/s00024-020-02515-y.

Carey, S., Sigurdsson, H., Mandeville, C., & Bronto, S. (2000). Volcanic hazards from pyroclastic flow discharge into the sea: Examples from the 1883 eruption of Krakatau, Indonesia. *Geological Society of America Special Publication, 345*, 1–14. https://doi.org/10.1130/0-8137-2345-0.1.

Choi, B. H., Pelinovsky, E., Kim, K. O., & Lee, J. S. (2003). Simulation of the trans-oceanic tsunami propagation due to the 1883 Krakatau volcanic eruption. *Natural Hazards and Earth System Sciences, 3*, 321–332. https://doi.org/10.5194/nhess-3-321-2003.

De Blasio, F. V., Elverhøi, A., Issler, D., Harbitz, C. B., Bryn, P., & Lien, R. (2005). On the dynamics of subaqueous clay rich gravity mass flows—The giant Storegga slide, Norway. In *Ormen lange—An integrated study for safe field development in the Storegga submarine area* (pp. 179–186). Elsevier. 10.1016/B978-0-08-044694-3.50019-6.

Fine, I. V., Rabinovich, A. B., Thomson, R. E., & Kulikov, E. A. (2003). Numerical modeling of tsunami generation by submarine and subaerial landslides. In A. C. Yalciner, E. N. Pelinovsky, C. E. Synolakis, E. Okal (Eds.), *Submarine Landslides and Tsunamis*, NATO Adv. Series (pp. 69–88). Dordrecht: Kluwer Acad. Publ. https://doi.org/10.1007/978-94-010-0205-9_9.

Francis, P. W. (1985). The origin of the 1883 Krakatau tsunamis. *Journal of Volcanology and Geothermal Research, 25*, 349–363. https://doi.org/10.1016/0377-0273(85)90021-6.

Giachetti, T., Paris, R., Kelfoun, K., & Ontowirjo, B. (2012). Tsunami hazard related to a flank collapse of Anak Krakatau Volcano, Sunda Strait, Indonesia. *Geological Society, London, Special Publications, 361*(1), 79–90. https://doi.org/10.1144/SP361.7.

Grilli, S. T., Tappin, D. R., Carey, S., et al. (2019). Modelling of the tsunami from the December 22, 2018 lateral collapse of Anak Krakatau volcano in the Sunda Straits, Indonesia. *Scientific Reports, 9*(1), 1–13. https://doi.org/10.1038/s41598-019-48327-6.

Heidarzadeh, M., Ishibe, T., Sandanbata, O., Muhari, A., & Wijanarto, A. B. (2020). Numerical modeling of the subaerial landslide source of the 22 December 2018 Anak Krakatoa volcanic tsunami, Indonesia. *Ocean Engineering, 195*, 106733. https://doi.org/10.1016/j.oceaneng.2019.106733.

Heidarzadeh, M., Muhari, A., & Wijanarto, A. B. (2018). Insights on the source of the 28 September 2018 Sulawesi tsunami, Indonesia based on spectral analyses and numerical simulations. *Pure and Applied Geophysics, 176*(1), 25–43. https://doi.org/10.1007/s00024-018-2065-9.

Horspool, N., Pranantyo, I., Griffin, J., et al. (2014). A probabilistic tsunami hazard assessment for Indonesia. *Natural Hazards and Earth System Sciences, 14*(11), 3105–3122. https://doi.org/10.5194/nhess-14-3105-2014.

Huang, X., & Garcia, M. H. (1998). A Herschel-Bulkley model for mud flow down a slope. *Journal of Fluid Mechanics, 374*, 305–333. https://doi.org/10.1017/S0022112098002845.

Imran, J., Harff, P., & Parker, G. (2001). A numerical model of submarine debris flow with graphical user interface. *Computers & Geosciences, 27*(6), 717–729. https://doi.org/10.1016/S0098-3004(00)00124-2.

Jiang, L., & LeBlond, P. H. (1993). Numerical modeling of an underwater Bingham plastic mudslide and the waves which it generates. *Journal of Geophysical Research: Oceans, 98*(C6), 10303–10317. https://doi.org/10.1029/93JC00393.

Latter, J. N. (1981). Tsunamis of volcanic origin: Summary of causes with particular references to Krakatoa, 1883. *Bulletin Volcanologique, 44*(3), 467–490. https://doi.org/10.1007/BF02600578.

Løvholt, F., Glimsdal, S., Harbitz, C. B., et al. (2014). Global tsunami hazard and exposure due to large co-seismic slip. *International Journal of Disaster Risk Reduction, 10*, 406–418. https://doi.org/10.1016/j.ijdrr.2014.04.003.

Maeno, F., & Imamura, F. (2011). Tsunami generation by a rapid entrance of pyroclastic flow into the sea during the 1883 Krakatau eruption, Indonesia. *Journal of Geophysical Research: Solid Earth, 116*, B09205. https://doi.org/10.1029/2011JB008253.

Mikami, T., Shibayama, T., Esteban, M., et al. (2019). Field Survey of the 2018 Sulawesi Tsunami: Inundation and run-up heights and damage to coastal communities. *Pure and Applied Geophysics, 176*, 3291–3304. https://doi.org/10.1007/s00024-019-02258-5.

Muhari, A., Heidarzadeh, M., Susmoro, H., et al. (2019). The December 2018 Anak Krakatau Volcano tsunami as inferred from post-tsunami field surveys and spectral analysis. *Pure and Applied Geophysics, 176*(12), 5219–5233. https://doi.org/10.1007/s00024-019-02358-2.

Nomanbhoy, N., & Satake, K. (1995). Generation mechanism of tsunamis from the 1883 Krakatau eruption. *Geophysical Research Letters, 22*(4), 509–512. https://doi.org/10.1029/94GL03219.

Omira, R., Dogan, G. G., Hidayat, R., et al. (2019). The September 28th, 2018, tsunami in Palu-Sulawesi, Indonesia: A post-event field survey. *Pure and Applied Geophysics, 176*(4), 1379–1395. https://doi.org/10.1007/s00024-019-02145-z.

Omira, R., Quartau, R., Ramalho, I., Baptista, M. A., & Neil, M. (2016). The tsunami effects of a collapse of a volcanic island on a semi-enclosed basin: The Pico-São Jorge channel in the Azores archipelago. In J. Duarte, W. Schellart (Eds.), *Plate boundaries and natural hazards,* American Geophysical Union (AGU) (pp. 271–283). Wiley. https://doi.org/10.1002/9781119054146.ch13 **(ISBN: 978-1-119-05397-2)**.

Paris, A., Heinrich, P., Paris, R., & Abadie, S. (2020). The December 22, 2018 Anak Krakatau, Indonesia, landslide and tsunami: Preliminary modeling results. *Pure and Applied Geophysics, 177*(2), 571–590. https://doi.org/10.1007/s00024-019-02394-y.

Paris, R. (2015). Source mechanisms of volcanic tsunamis. *Philosophical Transactions of the Royal Society A: Mathematical, Physical and Engineering Sciences, 373*(2053), 20140380. https://doi.org/10.1098/rsta.2014.0380.

Paris, R., Switzer, A. D., Belousova, M., et al. (2014). Volcanic tsunami: A review of source mechanisms, past events and hazards in Southeast Asia (Indonesia, Philippines, Papua New

Guinea). *Natural Hazards, 70*(1), 447–470. https://doi.org/10.1007/s11069-013-0822-8.

Prasetya, G., Husrin, S., Kongko, W., et al. (2019). The 22nd December 2018 Anak Krakatau Tsunami in Sunda Straits, Indonesia. In *Geophysical research abstracts* (Vol. 21). EGU2019-12276.

Putra, P. S., Aswan, A., Maryunani, K. A., Yulianto, E., Nugroho, S. H., & Setiawan, V. (2020). Post-event field survey of the 22 December 2018 Anak Krakatau tsunami. *Pure and Applied Geophysics*. https://doi.org/10.1007/s00024-020-02446-8.

Skvortsov, A., & Bornhold, B. (2007). Numerical simulation of landslide-generated tsunamis with application to the 1975 failure in Kitimat Arm, British Columbia, Canada. *Journal of Geophysical Research: Earth Surface, 112*, F02028. https://doi.org/10.1029/2006JF000499.

Socquet, A., Hollingsworth, J., Pathier, E., & Bouchon, M. (2019). Evidence of supershear during the 2018 magnitude 7.5 Palu earthquake from space geodesy. *Nature Geoscience, 12*(3), 192–199. https://doi.org/10.1038/s41561-018-0296-0.

Takabatake, T., Shibayama, T., Esteban, M., et al. (2019). Field survey and evacuation behaviour during the 2018 Sunda Strait tsunami. *Coastal Engineering Journal, 61*(4), 423–443. https://doi.org/10.1080/21664250.2019.1647963.

Thomson, R. E., Rabinovich, A. B., Kulikov, E. A., Fine, I. V., & Bornhold, B. D. (2001). On numerical simulation of the landslide-generated tsunami of November 3, 1994 in Skagway Harbor, Alaska. In G. Hebenstreit (Ed.), *Tsunami research at the end of a critical decade* (pp. 243–282). Dordrecht: Kluwer Acad. Publ. https://doi.org/10.1007/978-94-017-3618-3_17.

Titov, V., Rabinovich, A. B., Mofjeld, H. O., Thomson, R. E., & González, F. I. (2005). The global reach of the 26 December 2004 Sumatra tsunami. *Science, 309*(5743), 2045–2048. https://doi.org/10.1126/science.1114576.

Walter, T. R., Haghighi, M. H., Schneider, F. M., et al. (2019). Complex hazard cascade culminating in the Anak Krakatau sector collapse. *Nature Communications, 10*(1), 1–11. https://doi.org/10.1038/s41467-019-12284-5.

Williams, R., Rowley, P., & Garthwaite, M. C. (2019). Reconstructing the Anak Krakatau flank collapse that caused the December 2018 Indonesian tsunami. *Geology, 47*(10), 973–976. https://doi.org/10.1130/G46517.1.

Yokoyama, I. (1987). A scenario of the 1883 Krakatau tsunami. *Journal of Volcanology and Geothermal Research, 34*, 123–132. https://doi.org/10.1016/0377-0273(87)90097-7.

(Received May 13, 2020, revised June 5, 2020, accepted June 6, 2020)